CONF-9304144--14

LASER ABLATION OF GRAPHITE IN DIFFERENT BUFFER GASES

A. A. Puretzky*, D. B. Geohegan, R. E. Haufler, R. L. Hettich,
X.-Y. Zheng, and R. N. Compton

*Institute of Spectroscopy, Russian Academy of Sciences, 142092 Troitsk
Moscow, Russia
Oak Ridge National Laboratory, Oak Ridge, Tennessee

ABSTRACT

The KrF-laser ablation of graphite into 300 Torr of He, Ne, Ar, and Xe has been studied by fast imaging of the plasma emission and post-deposition analyses of collected film deposits. In each case, the soot which was redeposited on the irradiated rod following ablation was highly fullerene-deficient compared to the material collected on the sample disk 1.5 cm from the rod, as determined by laser desorption Fourier Transform Mass Spectrometry (FTMS)

Investigation of the plasma plume propagation using fast ICCD photography reveals three main phases to the expansion: (1) forward motion, deceleration and stopping of the leading edge of the plume, (2) an apparent reflected shock within the plume which propagates backward and reflects from the rod surface, (3) coalescence of these two components, resulting in continued expansion and dissipation of the plasma and the appearance of glowing ultrafine particles. For the laser plume propagating in 300 Torr of Xe the characteristic time intervals for these three phases are 0–300 ns, 300–1000 ns, and 1–1000 μs for phases (1), (2), and (3) respectively. The possible explanation of the observed difference in fullerene content is discussed on the basis of different plasma phases resulting in soot deposition on the rod and sample disk.

The measurement of ro-vibrational spectra of electronically excited C_2 has been performed. Rotational and vibrational temperatures, $T_R = 3000 \pm 300$K and $T_V = 6000 \pm 500$K have been obtained from the comparison of measured and calculated C_2 -Swan band emission.

INTRODUCTION

The original and, to date, most versatile method of producing fullerenes and doped fullerenes involves laser ablation of graphite into inert gas atmospheres.[1–5] Fullerenes and other clusters are formed during the thermalization of the hot plasma plume by a background gas, however the dynamics and mechanisms of this process are not well characterized or understood. In this work we report a number of experimental studies designed to provide insight into the mechanisms of fullerene growth in the laser plume.

These studies impact film growth by pulsed laser deposition (PLD), since ablation for PLD is often performed in background gases (however at much lower pressures ~ 200 mTorr) where an understanding of the slowing and scattering of the plume is also necessary. At the high background pressures used for this study, several effects suspected to occur in PLD plumes become observable by ICCD imaging, including the redeposition of material on the target surface, reflected shocks within the plume, and details of the plume coalescence.

A remarkable difference has been found between the fullerene content in the soot found on a collection disk (located 1.5 cm from the target) and the redeposited soot on the graphite rod target. No fullerene was detected in the soot redeposited onto the target rod surface when Ar and Xe were used as buffer gases. Only trace amounts of C_{60} were detected for He and Ne. However, the soot deposited on the sample disk was fullerene

enriched. This remarkable difference in fullerene content may be explained by the different plasma dynamics leading to soot deposition on the target rod and the sample disk.

EXPERIMENTAL

Three different kinds of experiments have been carried out in order to characterize the fullerene growing in the laser produced plasma plume. They are (1) soot deposition experiments followed by FTMS analysis of the produced material. (2) investigation of the laser plume propagation by two-dimensional images of the plume with fast intensified CCD camera and (3) spectroscopic study of C_2 visible luminescence.

The soot deposition was made in stainless steel chamber which was pumped out to 10^{-6} Torr and filled with a buffer gas. The pressure of the buffer gas was 300 Torr. Laser ablation was performed by focused beam of KrF-laser (λ= 248 nm, 30-ns FWHM, 2×2 mm^2 image on the rod surface, fluence = 20 J/cm^2) incident at 30° to the normal. The graphite rod was rotated by a motorized feedthrough. The geometry for this experiment as well as for imaging of the plume is diagrammed in the upper left-hand corner in Fig. 3. The 16.5 mm -stainless steel sample disk for FTMS was located in front of the laser plume at 15.4 mm from the rod surface. The repetition rate of the pulsed laser was 5 Hz and irradiation time for all four buffer gases used was 30 minutes. The analysis of the ablated material was performed with an Extrel FTMS-2000 Fourier Transform Mass Spectrometer equipped with a Quanta Ray DCR-11 Nd:YAG pulsed laser. The laser was operated at 355 nm and focused to approximately 10^7–10^8 W/cm^2 in order to desorb and ionize the sample deposited on the disk. A fixed number of pulses from the desorption laser simultaneously evaporated and ionized molecular species present on the sample disk. These ions were subsequently trapped, manipulated and detected in the cell of the FTMS. Both positive and negative ions were examined. For most experiments the ions were trapped for 3 – 20 ms at a background pressure of 8×10^{-8} Torr prior to their detection.

The experimental apparatus for gated – ICCD photography has been previously described.[6] A lens-coupled, gated-intensified, CCD-array camera (Princeton Instruments ICCD–576G/RB with 105 mm Nikkor-UV lens) was responsive over a 200–820 nm wavelength range. A rotating carbon rod was viewed side-on following irradiation by 20 J/cm^2 KrF laser pulses. The camera was gated by variable-width voltage pulses applied to the microchannel plate, resulting in "shutter speeds" $\geq$ 5 ns.

The spectral analysis of the laser plume emission from the laser ablated graphite was recorded with a monochromator equipped with a photomultiplier. The time profile of the spacially selected plume emission could be studied by a gated detector (boxcar integrator) synchronized to the laser firing.

RESULTS AND DISCUSSION

Figure 1 shows FTMS spectra (positive ions) of the brownish colored soot deposited 1.5 cm from the target onto the sample disk through 300 Torr of He, Ne, Ar, and Xe gas. The amount of soot collected under the same conditions was largest for He and smallest for Xe. Pronounced C_{60} , C_{70} as well as other fullerene peaks are observed in these spectra. The quantitative comparison of the absolute amount of the C_{60}, C_{70} for the used buffer gases shows that He and Xe give the highest yield of fullerene compared to Ne and Ar. Another interesting feature of these mass spectra is the shift of the fullerene distribution to the higher masses for Xe compared to He.

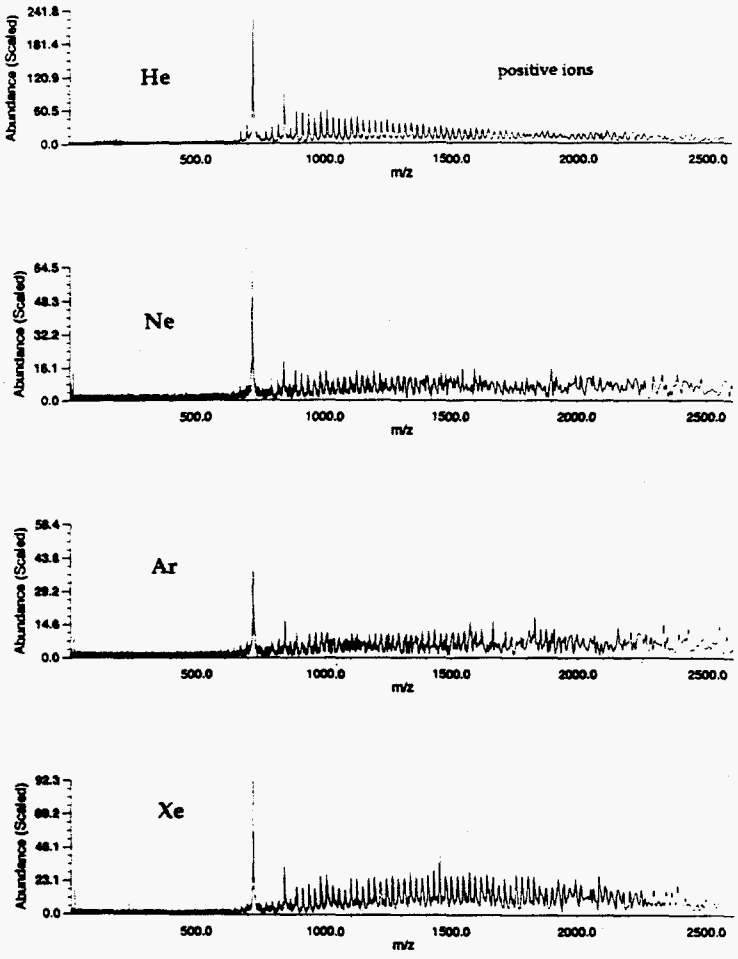

Fig. 1. FTMS spectra of the soot deposited on the 16.5 mm sample disk located in front of the laser plume at 15.4 mm from the irradiated graphite rod surface. The pressure of the buffer gases was 300 Torr. The relative abundances are approximate.

The KrF-laser irradiation of the graphite rod also resulted in the redeposition of large amounts of black colored soot (compared to the brownish colored material deposited on the sample disk) onto the side surface of the graphite target rod. The soot produces a cylindrical black band a few millimeters in width starting from the front edge of the graphite rod. The largest bands were formed for Xe and Ar and much less redeposited material was found for He and Ne. This redeposited soot was collected from the target rod and figure 2 presents the FTMS spectra (positive ions) obtained for this material.

Only trace amounts of C_{60} were found in the redeposited soot when He and Ne were used as buffer gases. As shown in Fig. 2, C_{60} was not found in the redeposited material for Ar and Xe. In addition, there are no higher-mass fullerenes (up to m/z = 2000) in the spectra.

We have also made Scanning Electron Microscopy (SEM) images of the soot deposited back onto the rod. A broad distribution of particle sizes ranging from 10 nm to 1 μm (comprised of coalesced smaller particles) can be found in these pictures.

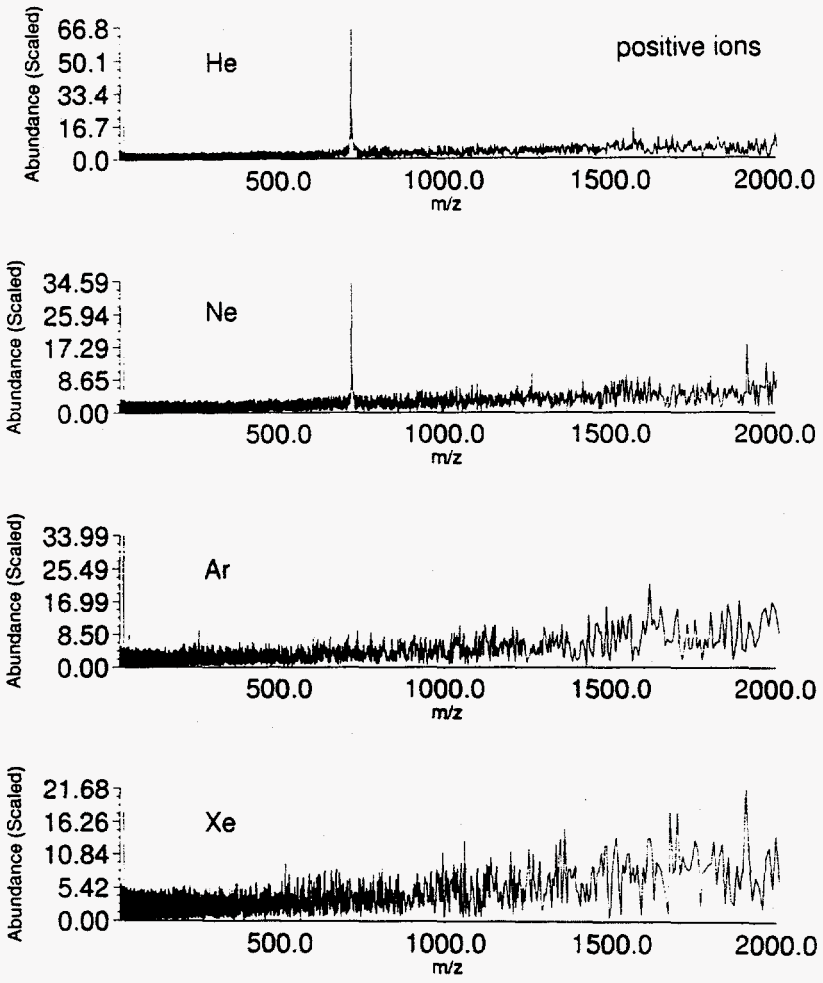

Fig. 2. FTMS Spectra of the soot redeposited onto the side of the graphite rod. The abundance scales are relative and not to be compared with those in Figure 1.

In order to understand the remarkable differences in fullerene content between the sample and the rod soot, we have studied the plasma propagation in various buffer gases (He, Ne, Ar, Xe). Figure 3(a)–3(c) shows the visible plasma emission from 10 ns to 1 ms following the onset of the KrF laser pulse as the plume expands into 300 Torr xenon gas. The exposures were varied over many orders of magnitude as the extremely bright plasma expanded and dimmed into the photon counting regime, following techniques recently applied to image hot particulates generated during vacuum ablation of YBCO and BN[10].

Three main phases of the laser plume evolution can be discerned in Fig. 3. The three phases can be categorized as (1) initial expansion and stopping of the plasma, (2) reflection, backward movement, and redeposition, and (3) reflection from the target face,

plume coalescence and subsequent expansion. The first phase takes time from 0 to 1000 ns, where the plume expands into the background gas and is slowed until nearly 'stopped'. At t = 300 ns, however, a second well-pronounced phase starts. A portion of the plasma appears to reflect from the slowed contact front of the expanding plasma

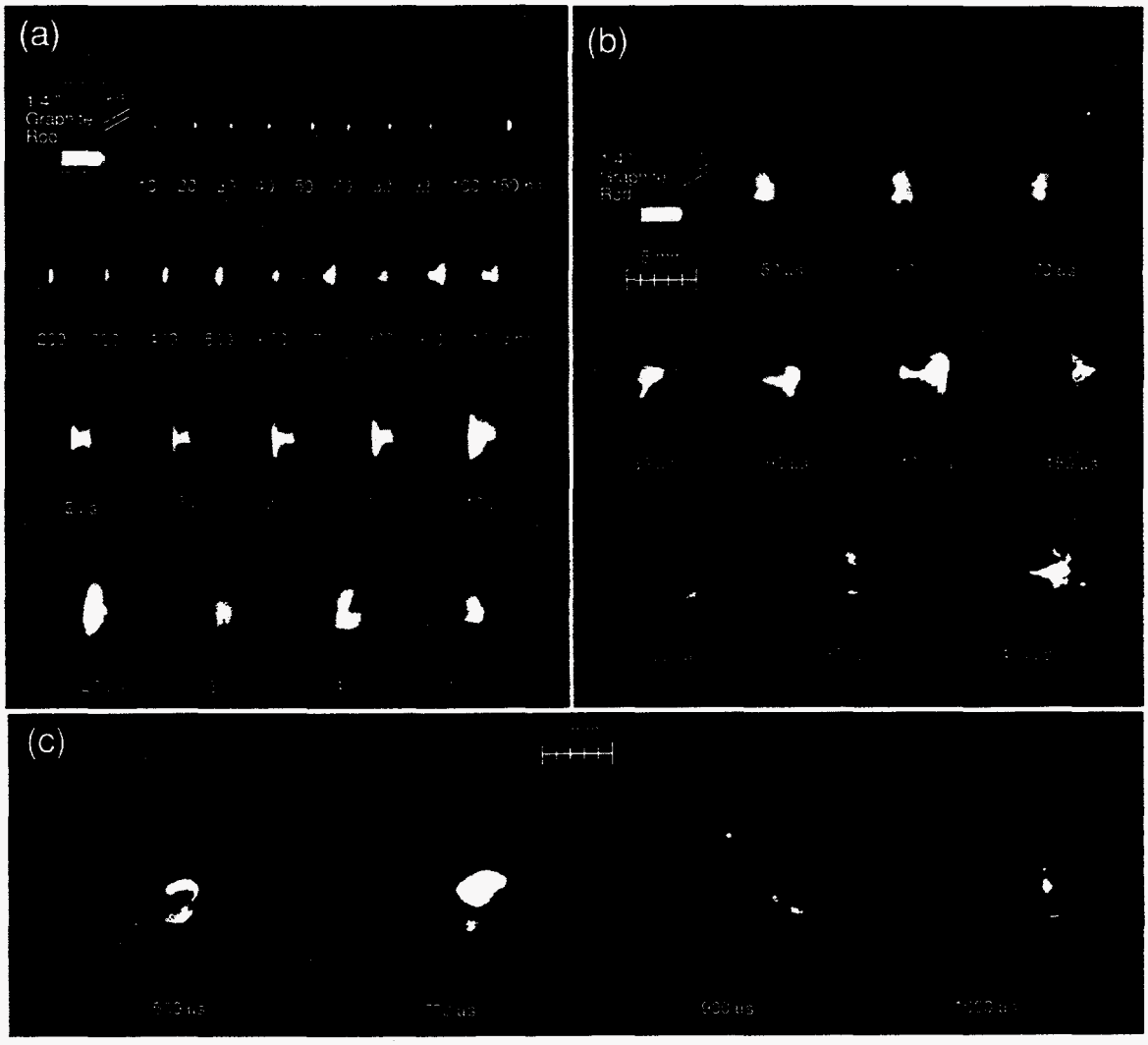

Fig. 3. ICCD photographs of the visible plasma emission following 20 J/cm^2 KrF-laser ablation into 300 Torr of Xe. The 0.2 × 0.2 cm^2 248-nm laser pulse irradiated the graphite rod at an angle of 30° from the normal. The gate widths range from 5ns to 2 μs.

bubble, and then move backward toward the target rod surface. At t = 600 ns this reflected component reaches the rod face and spreads over the surface. The backward-moving plasma also wraps around the side surface of the rod, starting the 'redeposition' of the soot which was collected for Figure 2 above. The images show that the plasma engulfs the rod for a period extending only to about 20 μs, presumably leading to

redeposition of material on the rod for this period of time. The third phase of the expansion begins after $\Delta t \sim 600$ ns when a portion of the backward-moving component of the plasma bubble reflects from the rod surface and begins to move out to join the 'stopped' material. The third phase is most noticeable after $\Delta t > 2$ μs, as this material moves to coalesce with the remainder of the plume around $\Delta t \approx 10$ μs. Together, the plume appears to move again into the buffer gas, as shown in Figure 3(a) and 3(b) for $\Delta t > 10$ μs . This third phase of plume propagation is observable up to $\Delta t \sim 1$ ms. Incidentally, although the images shown in Figure 3 were each taken for a different laser shot and exposure, the size and shape of the plume were remarkably reproducible from shot to shot up to time delays of ~ 300 μs where turbulent behavior became unpredictable.

At later times [Fig. 3(c)], the turbulent motion of ultrafine particles appears to become observable once the plasma emission has diminished sufficiently. The ultrafine particles are relatively hot, so they emit visible blackbody radiation which can be detected by spectroscopy and ICCD photography.[2,10] The emission from the hot particles occupies a spatial region which is separated by several millimeters from the target surface, extending out to where the sample deposits of Figure 2 were collected. Missing from these images are the profusion of hot, slow-moving larger particles which were noted in Ref. 10 for YBCO and BN. An occasional streaking 'large' particle was occasionally noted during the imaging, with velocity $\sim 1.6 \times 10^3$ cm/s which could be estimated from the length of the image and the gate width. Extremely faint images of emission near the target surface may imply that some hot clusters are emitted from the target at very late times, however.

Measurement of the front edge of the laser plume as a function of time permits one to estimate initial velocities and stopping distances of the plume. This data is used to test different models which are widely used for a plasma propagation in surrounding media.[7,8]

Details of such plasma propagation can be found in Ref. [6]. For the drag model the position of the front edge, x , of the plume is given by Eq. (1):

$$x = x_f [1-\exp(-\beta t)] \tag{1}$$

where X_f is the stopping distance of the front edge of the plume and β is the slowing coefficient. For the shock wave propagation model we have

$$x = \xi_0 \left(\frac{E_0}{\rho_0} \right)^{1/5} t^a \tag{2}$$

were ξ_0 is a constant, E_0 is the explosive energy, ρ_0 is the density of background gas and $\alpha = 0.4$ for a spherical expansion.

Figure 4 shows the measured plume position (leading edge along the target normal) versus time for 20 J/cm^2 KrF-laser ablation of graphite into 300 Torr of He, Ne, Ar, and Xe as measured from sets of ICCD photographs. The drag model fits the experimental data in the time interval from 0 to 1 μs. Table 1 gives initial velocities and the fitting parameters for the models (1) and (2).

The observed propagation of the laser plume into surrounding buffer gases can be summarized as follows. The laser beam creates a plasma with a front-edge propagation velocity about 1.4×10^6 cm/s (Table 1). This is at least one order of magnitude higher

than the sound velocity in the surrounding buffer gas. This plasma contact front locally compresses the surrounding buffer gas until the pressure inside plasma bubble reaches that of the locally compressed buffer gas. During this process, a reflected shock is generated within the plasma bubble which moves in the opposite direction until it reaches the rod surface. This shock wave travels within the plume material, collides and reflects from the rod, and propagates with lower velocity into the buffer gas.

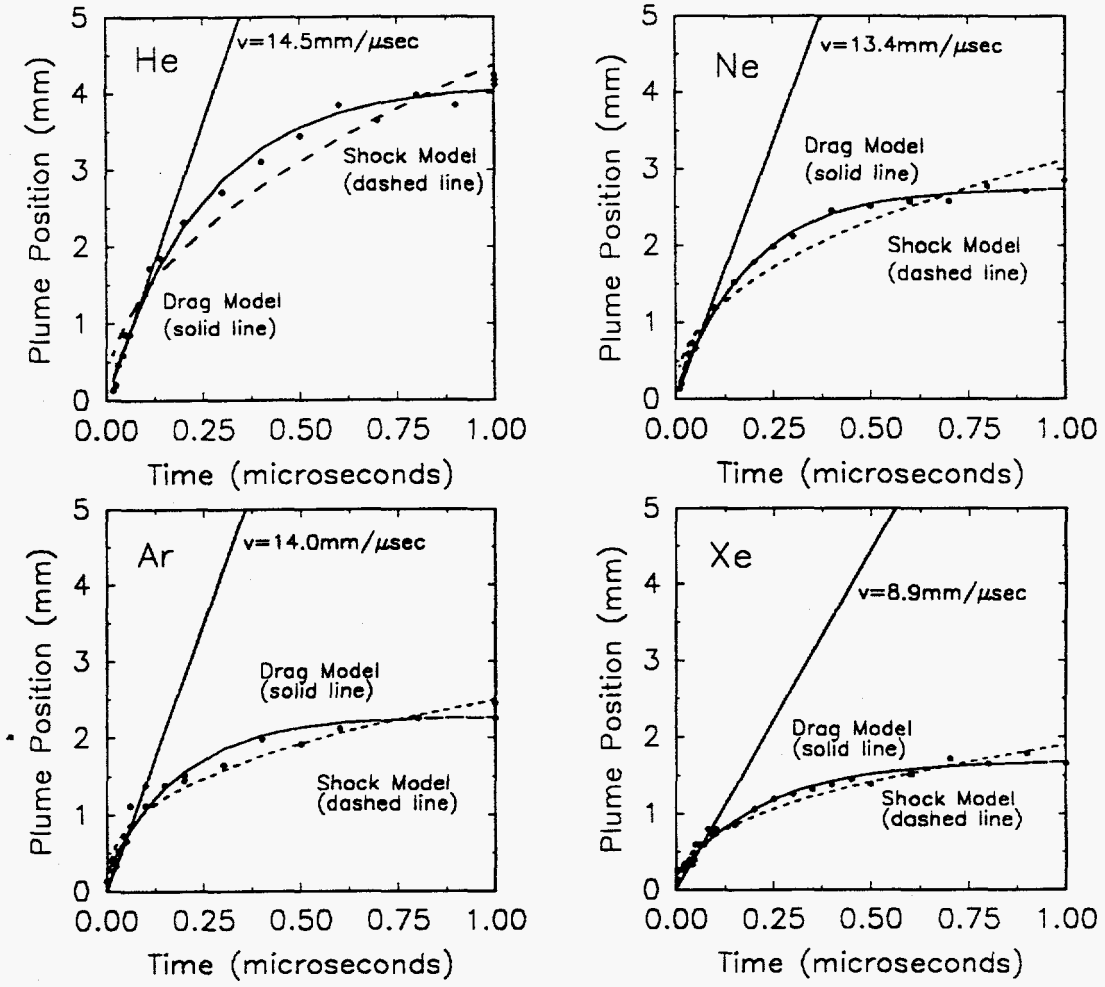

Fig. 4. Plume position (leading edge along the target normal) versus time for 20 J/cm^2 KrF-laser ablation of graphite into 300 Torr of He, Ne, Ar, and Xe as measured from sets of ICCD photographs. Curve fitting results from the *drag model* (solid line) and the *shock wave propagation model* (dashed line) are given for the 0–1.0 μs phase of the expansion.

Model		units	Helium	Neon	Argon	Xenon
Drag	x_f	mm	4.1	2.7	2.0	1.5
	β	1/μsec	4.0	5.1	5.3	4.3
Shock wave	α	mm	4.4	3.1	2.5	1.9
	α		0.49	0.43	0.37	0.42
Initial velocity	υ	mm/μsec	14.5	13.4	14.0	8.9

Table 1. Fitting parameters for the data of Figure 4 using the *drag* and *shock wave* propagation models.

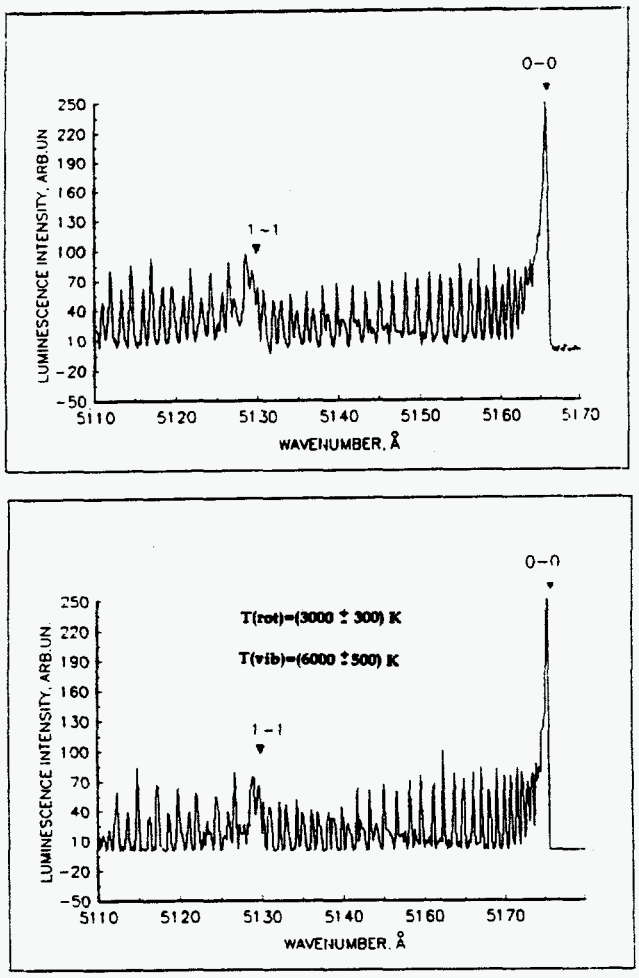

Fig. 5. Experimental (top) and simulated (bottom) emission spectrum of C_2 in the laser plume in 300 Torr of He ($\Delta v = 0$, Swan band) from 5110 Å to 5180 Å. The gate width was 4 μs.

The difference in fullerene content between the material deposited on the rod and on the sample disk may be rationalized if one takes into account that disk soot deposition occurs after 500–1000 μs (the third phase) when the ablated material is cooled and mixed well with the buffer gas.

The soot deposited on the rod consists of ultrafine particles which either condensed from atomic vapor during the redeposition process or evaporated from the rod. The backward plasma results in the deposition of this material on the rod surface. A fraction of the backward-moving material reflects from the rod surface and travels with the long-lived plasma, anneals, and gives rise to fullerene growth. These growing clusters finally deposit on the sample disk.

The rotational and vibrational temperatures of electronically excited C_2 were determined by comparison of the measured spectra with those calculated using the rotational-vibrational constants given in Ref. 9. Figure 5 shows an example of the experimental (buffer gas He) and calculated spectra for the sequence $\Delta\upsilon = 0$ of the Swan band. The simulation of the experimental spectrum gives $T_{rot} = 3000 \pm 300$K and $T_{vib} = 6000 \pm 500$K. Emission from C_2^* was the main source of radiation although C_2^- and blackbody radiation were also detected.

CONCLUSIONS

The KrF-laser ablation of graphite rod in 300 Torr of He, Ne, Ar, and Xe produces two different kinds of soot. The soot deposited on the side surface of the graphite rod was fullerene deficient for all buffer gases used. The ablated material collected on the sample disk contains fullerenes whose mass distribution depends on the buffer gas used.

The laser plume propagation study reveals three different phases in the plasma "bubble" time evolution: (1) initial expansion and 'stopping' of the plasma, (2) reflection, backward movement, and redeposition, and (3) reflection from the target face, plume coalescence and subsequent expansion into the buffer gas.

The remarkable difference observed between the fullerene content in the soot deposited on the rod and on the sample disk can be rationalized by the time spent in the laser plasma before deposition. The observation of "hot" ultrafine particles in the buffer gas well after the plasma has decayed raises questions as to its importance in fullerene growth and annealing.

ACKNOWLEDGMENTS

REH acknowdeges support by an appointment to the U. S. Department of Energy Laboratory Cooperative Postgraduate Research Training Program administered by the Oak Ridge Institute for Science and Education. This publication was based upon research sponsored by the Directors R&D Fund at Oak Ridge National Laboratory, and the Office of Health and Environmental Research and the Division of Materials Sciences, U.S. Department of Energy, under contract DE-AC05-84OR21400 with Martin Marietta Energy Systems, Inc..

REFERENCES

1. H. W. Kroto, J. R. Heath, S. C. O'Brien, R. F. Curl, and R. E. Smalley, *Nature* **318**, 162 (1985).
2. E. A. Rohlfing, D. M. Cox, A. Kaldor, *J. Chem. Phys.* **81**, 3322 (1984).
3. R. E. Haufler, Y. Chai, L. P. F. Chibante, J. Conceicao, C. Jin, L.-S. Wang, S. Maruyama, R. E. Smalley, *Mater. Res. Soc. Symp. Proc.* **206**, 627 (1990).

4. Y. Chai, T. Guo, C. Jin, R. E. Haufler, L.P.F. Chibante, J. Fure, L. Wang, J. M. Alford, R. E. Smalley, *J. Phys. Chem.* **95**, 7564 (1991).
5. T. Guo, C. Jin, R. E. Smalley, *J. Phys. Chem.* **95**, 4948 (1991).
6. D. B. Geohegan, *Appl. Phys. Lett.*, **60**, 2732 (1992).
7. P. E. Dyer, A. Issa, and P. H. Key, *Appl. Surf. Sci.* **46**, 89 (1990); *Appl. Phys. Lett.* **57**, 186 (1990).
8. Ya. B. Zel'dovich and Yu. P. Raizer, in *Physics of Shock Waves and High Temperature Hydrodynamic Phenomena* (Acaemic, New York, 1966), Vol. **1**, p. 94.
9. J. G. Phillips and S. P. Davis, *Berkeley Analyses of Molecular Spectra* (Univ. of California Press., Berkeley 1968) Vol. **2**, p. 1–187.
10. D. B. Geohegan, this proceedings, and *Appl. Phys. Lett.*, **62**, 1463 (1993).